



# Superimposed effects of typical local circulations driven by mountainous topography and aerosol-radiation interaction on heavy haze in the Beijing-Tianjin-Hebei central and southern plains in winter

5 Yue Peng<sup>1</sup>, Hong Wang<sup>1</sup>, Xiaoye Zhang<sup>1,2</sup>, Zhaodong Liu<sup>1</sup>, Wenjie Zhang<sup>1</sup>, Siting Li<sup>1</sup>, Chen Han<sup>1</sup>,  
Huizheng Che<sup>1</sup>

<sup>1</sup>State Key Laboratory of Severe Weather (LASW) & Key Laboratory of Atmospheric Chemistry of China Meteorological Administration, Chinese Academy of Meteorological Sciences (CAMS), Beijing, 100081, China

<sup>2</sup>Center for Excellence in Regional Atmospheric Environment, IUE, Chinese Academy of Sciences, Xiamen, 361021, China

10 *Correspondence to:* Hong Wang (wangh@cma.gov.cn); Xiaoye Zhang (xiaoye@cma.gov.cn)

**Abstract.** Although China's air quality has substantially improved in recent years due to the vigorous emission reduction, the Beijing-Tianjin-Hebei (BTH) region, especially its central and southern plains at the eastern foot of the Taihang Mountains, has been the most polluted area in China with persistent and severe haze in winter. Combining meteorology-chemistry coupled model simulations and multiple observations, this study explored the causes of several heavy haze events  
15 in this area in January 2017, focusing on local circulations related to mountain terrain. The study results showed that on weather scale, the configuration of the upper, middle, and lower atmosphere provided favorable weather and water vapor transport conditions for the development of haze pollution. Under the weak weather-scale systems, local circulation played a dominant role in the regional distribution and extreme values of PM<sub>2.5</sub>. Influenced by the Taihang and Yanshan Mountains, vertical circulations and wind convergence zone were formed between the plain and mountain slopes. The vertical  
20 distribution of pollutants strongly depended on the intensity and location of the circulation. Strong and low circulation was more unfavorable to the vertical diffusion and horizontal transport of near-surface pollutants. More importantly, we found that aerosol-radiation interaction (ARI) significantly amplified the impacts of local vertical circulations on heavy haze by two mechanisms. First, ARI strengthened the vertical circulations at the lower levels, with the zonal wind speeds increasing by 0.2–0.8 m s<sup>-1</sup>. Meanwhile, ARI could cause a substantial downward shift of the vertical circulations (~100 m). Second,  
25 ARI weakened the horizontal transport of pollutants by reducing the westerly winds below 300 m and enhancing the wind convergence below 1000 m. Under these two mechanisms, pollutants could only recirculate in a limited space. This superposition of typical local circulation and ARI eventually contributed to the accumulation of pollutants and the consequent deterioration of haze pollution in the region.



## 1 Introduction

30 China's air quality has considerably improved in recent years because of aggressive emission reduction measures (Zhang et al., 2019; Zheng et al., 2018). However, the large urban agglomeration such as BTH and the Yangtze River Delta (YRD) still frequently suffer from persistent heavy haze pollution and the deterioration of atmospheric visibility that it causes, especially in winter (Huang et al., 2020; Peng et al., 2020). Fine particulate matter ( $PM_{2.5}$ ) is the primary aerosol component of haze and a significant factor affecting visibility. During heavy haze pollution,  $PM_{2.5}$  concentrations often exceeded  $300 \mu\text{g m}^{-3}$ ,  
35 and sometimes even  $500 \mu\text{g m}^{-3}$  in these areas (Peng et al., 2021; Wang et al., 2018; Zhang et al., 2020). Under stable emissions, unfavorable meteorological conditions, particularly within the planetary boundary layer (PBL), are closely associated with the cumulative explosive growth of aerosols on haze pollution days.

Previous studies illustrated that there is a positive feedback between aerosols and the PBL: During heavy haze pollution, high aerosol concentrations weaken the turbulence in the lower troposphere mainly by scattering the solar radiation, thus  
40 inhibiting the development of PBL (Miao et al., 2019; Peng et al., 2021; Quan et al., 2013; Wang et al., 2018; Zhong et al., 2018a), while absorbing aerosols, such as black carbon (BC), can heat the upper PBL, and further enhance the stability of the atmospheric stratification (Ding et al., 2016; Huang et al., 2018). The decreased PBL associated with high concentration aerosols increases near-surface relative humidity (RH) by weakening the vertical transport of water vapor; the increased RH in turn promotes the formation of secondary aerosols (Li et al., 2017; Liu et al., 2018). These aerosol direct and semi-direct  
45 effects or ARI will eventually deteriorate haze pollution. In addition, aerosols can act as cloud condensation nuclei or ice nuclei, modifying cloud physical and radiative properties by participating in cloud microphysical processes, this aerosol-cloud interaction in turn affect the structure and development of the PBL (Zhang et al., 2015; Zhao et al., 2017).

In addition to the impacts of ARI on the PBL meteorology, local circulations driven by unique topography also play an important role in the variations of PBL structure as well as the spatial and temporal distribution of pollutants (Chen et al.,  
50 2009; Liu et al., 2009; Miao et al., 2015; Zhang et al., 2018). The BTH region is located in the North China Plain (NCP), with the Yanshan Mountains to the north, Taihang Mountains to the west, and the Bohai Sea to the east (Fig. 1a). The elevation difference between these two Mountains and the NCP can reach 1500–2000 m. Such a complex geographical environment makes the BTH region have unique local atmospheric circulation characteristics and is prone to local accumulation or regional transport of pollutants. Chen et al. (2009) found that the elevation of the pollution layer in Beijing  
55 is associated with the mountain-plain breeze, which causes a rapid increase of pollutants in the near-surface in this area. The intensity of local atmospheric circulation can strongly affect the removal and accumulation of local pollutants. In the absence of strong weather systems, the well-developed valley wind circulation and sea breeze circulation over the BTH region are conducive to the long-distance transport of pollutants (Miao et al., 2015). On the contrary, weak local circulations make pollutants recirculate in a limited space and accumulate continuously (Lo et al., 2006; Sun et al., 2013). In addition, several  
60 topographic sensitivity experiments have been conducted to examine their effects on the low-level circulation and PBL structure in the BTH (Wang et al., 2019; Zhang et al., 2018), and the results highlight the significance of topography in the



formation and accumulation of haze pollution. Despite the fact that there have been numerous previous studies on haze pollution in the BTH, most of them concentrated on the ARI and topographic effects separately, whereas studies on the combined effects of topography-induced local circulation and ARI on pollution (Miao et al., 2020), particularly the effects of ARI on local circulation are still scarce. Given the key role of the two-way feedback mechanism between aerosol and PBL on heavy pollution accumulation and the dominant role of local circulation on the pollutant distribution under weak weather systems, this study comprehensively analyzes the link between local circulation, ARI, and haze in BTH, especially the impacts of ARI on local circulation, using the online coupled atmospheric chemistry model GRAPES\_Meso5.1/CUACE.

## 2 Method and data

### 2.1 GRAPES\_Meso5.1/CUACE and experimental design

GRAPES\_Meso5.1/CUACE is an online regional atmospheric chemistry model designed for both operational and research applications. There are two major parts of this model: a weather model GRAPES\_Meso5.1 and a chemistry model CUACE. The former is a mesoscale weather prediction model that primarily consists of a fully compressible non-hydrostatic model core and a modularized physics package (Chen et al., 2008); the latter is an online chemistry model that is mainly composed of aerosol and gaseous chemistry modules with emission and dynamic processes (Gong and Zhang, 2008). Wang et al. (2022) established this updated model and provided a comprehensive description of the model. In this model, Peng et al. (2022) implemented the ARI mechanism for the two-way feedback between aerosols and weather processes by incorporating the real-time calculated aerosol optical parameters.

The model domain in this study is centered over the BTH region, covering an area of 33–45 °N in latitude and 110–125 °E in longitude (Fig. 1a). The model has a horizontal resolution of 10 km and 49 unevenly spaced vertical levels ranging from near-surface to 33 km. The physical configuration options selected in this study include the Thompson microphysics (Thompson et al., 2008), the KF cumulus scheme (Kain, 2004), the RRTMG longwave radiation scheme (Mlawer et al., 1997), the Goddard shortwave radiation scheme (Chou et al., 1998) including ARI mechanism, the MRF boundary layer scheme (Hong and Pan, 1996), the MM5 surface layer scheme (Zhang and Anthes, 1982) and Noah land surface scheme (Ek et al., 2003). The chemical configuration options mainly include an emissions inventory treatment system that can process the Multi-resolution Emission Inventory for China (MEIC) of 2017 (Zheng et al., 2018) adopted in this study into the format available for the model, the Second Generation Regional Acid Deposition Model (RADM2) gas-phase chemistry (Stockwell et al., 1990), and the CUACE aerosol model (Gong and Zhang, 2008; Wang et al., 2010, 2015a, 2015b).

The model simulation was conducted from December 29, 2016, to January 31, 2017, with a looping time of 72 h. The first 72 h simulations were considered the spin-up period. To evaluate the impacts of ARI, two numerical scenarios were performed in this study. The first is the controlling simulation (CTL) with the above configurations and ARI; the second is the sensitive experiment (EXP) which is consistent with CTL but does not consider ARI.



## 2.2 Data

Four categories of data was used in this study: The global Final analysis (FNL) data with a horizontal resolution of  $0.25^\circ \times$   
95  $0.25^\circ$  (<http://rda.ucar.edu/data/ds083.3/>) provided by the National Centers for Environmental Prediction (NCEP), which was  
used for the meteorology initial and lateral boundary fields of the model and the analysis of large-scale circulation in upper  
and middle levels; Multi-year climate average of chemical tracers used for chemistry initialization of the model (Wang et al.,  
2022); Hourly near-surface  $PM_{2.5}$  mass concentration measured by 149 state-controlled stations provided by the China  
National Environmental Monitoring Center (<http://www.cnemc.cn/>) and 210 stations provided by the Hebei Meteorological  
100 service; Vertical meteorology data for three sounding stations in BTH, i.e., Beijing (BJ), Tangshan (TS), and Xingtai (XT),  
including air pressure, temperature, and wind at 08:00 and 20:00 Beijing time (BJT) each day, measured by the L-band  
radiosonde system.

## 3 Results and discussion

### 3.1 Model performance

105 Accurate reproduction of aerosol concentration variations and the vertical structure of the atmosphere is a prerequisite for  
quantifying ARI (Zhang et al., 2015) as well as local circulation. Figure 1 shows the distribution of observed and simulated  
monthly mean  $PM_{2.5}$  concentrations in January 2017. The BTH region suffered from severe haze pollution in January 2017,  
with its regional monthly mean observed  $PM_{2.5}$  concentration reaching  $130 \mu g m^{-3}$ . Particularly at the eastern foot of the  
Taihang Mountains, the central and southern plains of BTH, the  $PM_{2.5}$  values exceeded  $200 \mu g m^{-3}$  and even  $250 \mu g m^{-3}$ .  
110 High anthropogenic emission coupled with a stable atmosphere due to the mountainous topography leads to frequent and  
severe haze events in this area (Fu et al., 2014). BTH is surrounded by the Yanshan and Taihang Mountains from north to  
west, and such topography is not conducive to pollutant dispersion since the mountains weaken the cold air from the north  
and west and block the transport of pollutants associated with easterly and southerly winds (Gao et al., 2017; Miao et al.,  
2015; Quan et al., 2020; Zhong et al., 2018b). The comparison of the observed and simulated  $PM_{2.5}$  results (Fig. 1c–d) shows  
115 that although both simulation scenarios reproduced the distribution of  $PM_{2.5}$  concentrations, the CTL results with ARI were  
closer to the observations. For the whole BTH region, the mean biases of the simulated results for CTL and EXP were  $-17$   
and  $-41 \mu g m^{-3}$ , respectively. For the most polluted central and southern BTH, the maximum  $PM_{2.5}$  concentration exceeded  
 $225 \mu g m^{-3}$  in CTL and was less than  $200 \mu g m^{-3}$  in EXP. This result not only demonstrates the applicability of the model,  
but also the need to consider ARI effects for pollutant simulation.

120

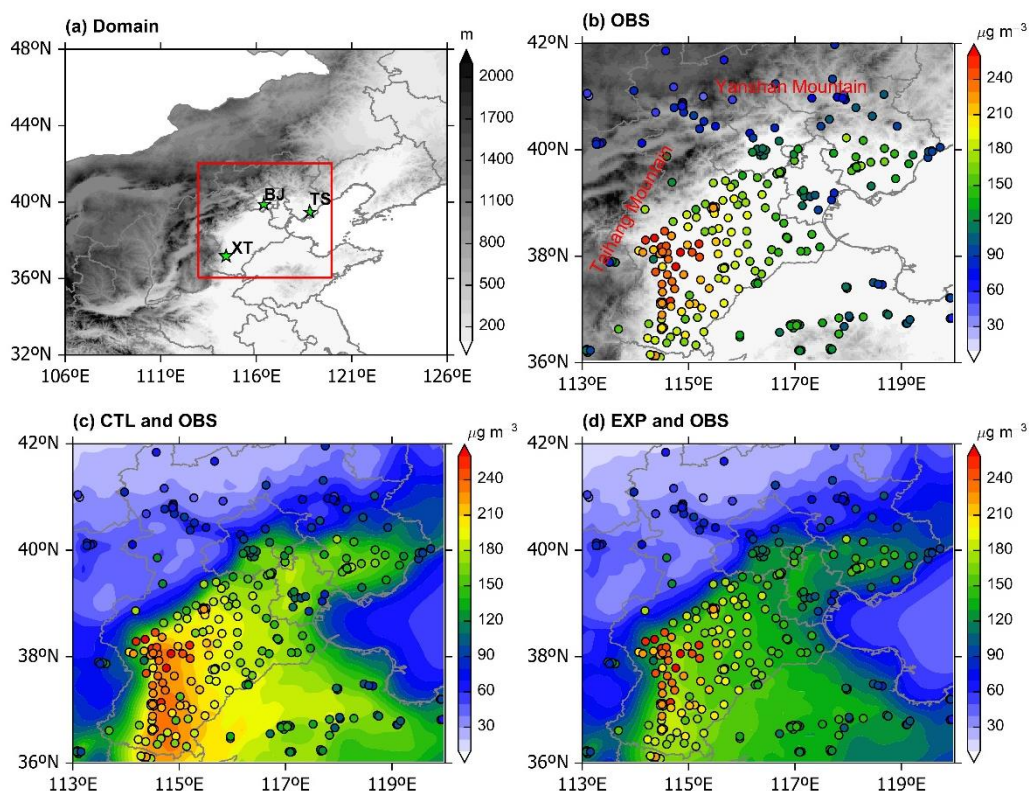
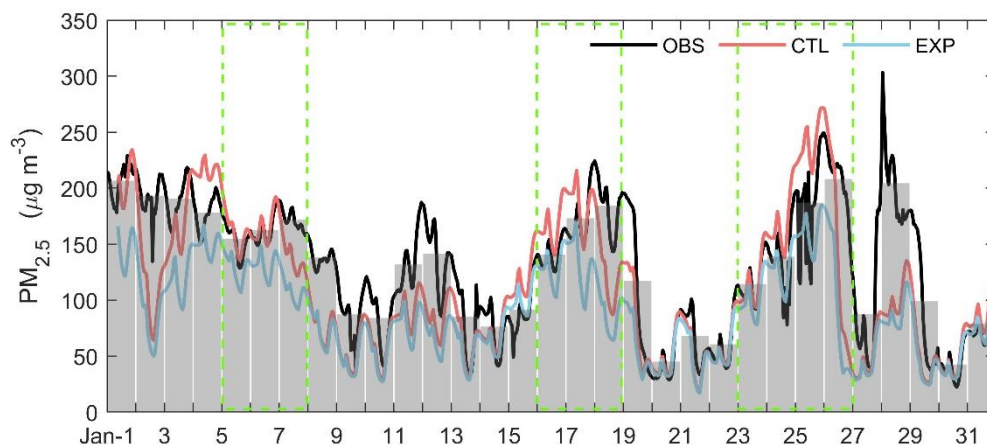


**Figure 1.** (a) Model domain (shading denotes terrain height; red rectangle shows the general location of BTH; green star denotes the weather sounding station) and (b–d) spatial distributions of observed and simulated PM<sub>2.5</sub> concentrations in January 2017.

125

The hourly variation of observed and simulated PM<sub>2.5</sub> concentrations in BTH was compared in Fig. 2. The model generally reproduced the temporal variation of observed PM<sub>2.5</sub>, with correlation coefficients of 0.74 and 0.71 for CTL and EXP, respectively. This result also demonstrated that the simulations of CTL were more consistent with observations, which significantly improved the underestimation of high PM<sub>2.5</sub> concentrations through the ARI mechanism. Given that the short-term characteristics of the local circulation have a greater influence on the extreme values of PM<sub>2.5</sub> than its long-term characteristics, representative pollution days will be selected for this study. As shown in Fig. 2, the BTH region suffered from several persistent heavy haze pollutions throughout the month, and the daily mean PM<sub>2.5</sub> concentrations kept climbing upward and exceeded 100 μg m<sup>-3</sup> on January 5–7, 16–18, and 23–26. Therefore, we finally selected January 6, 17, and 24 as the representatives of three pollution periods, considering the simulation results and PM<sub>2.5</sub> concentrations.

130

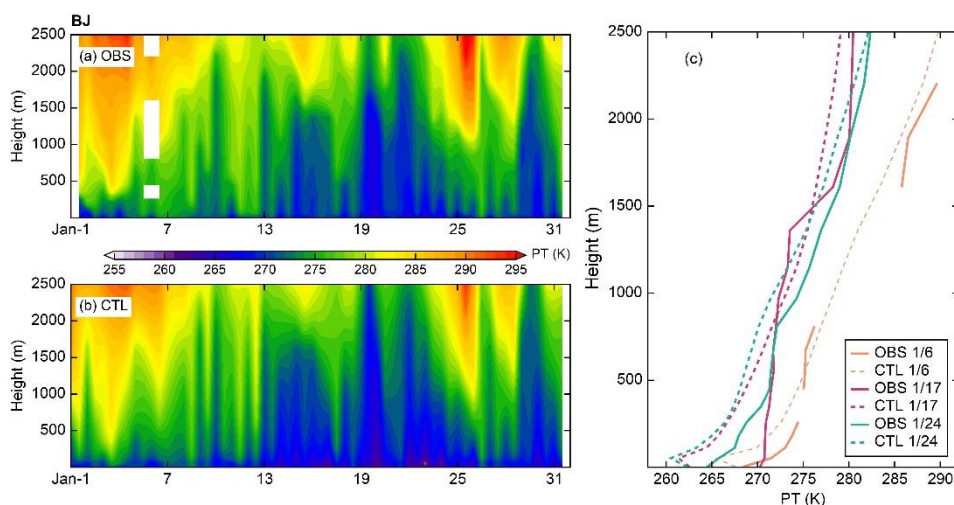


135

**Figure 2.** Time series of observed and simulated  $PM_{2.5}$  concentrations in BTH during January 2017. Grey bar: observed daily mean  $PM_{2.5}$  concentrations; Green box: pollution period.

Given the important influence of atmospheric vertical structure, especially temperature stratification, on the formation of pollutants, we further evaluated the model performance (CTL) in simulating the vertical profile of the potential temperature (PT) at BJ, TS, and XT by comparing sounding observations. As shown in Fig. 3, the model simulations reasonably reproduced the vertical distribution of temperature in BJ, TS, and XT, including a good simulation of atmospheric warming during the pollution period. For the three selected pollution days (January 6, 17, and 24), the correlation coefficients of PT below 2500 m were 0.83–0.99 in BJ, 0.96–0.99 in TS, and 0.90–0.99 in XT.

140



145

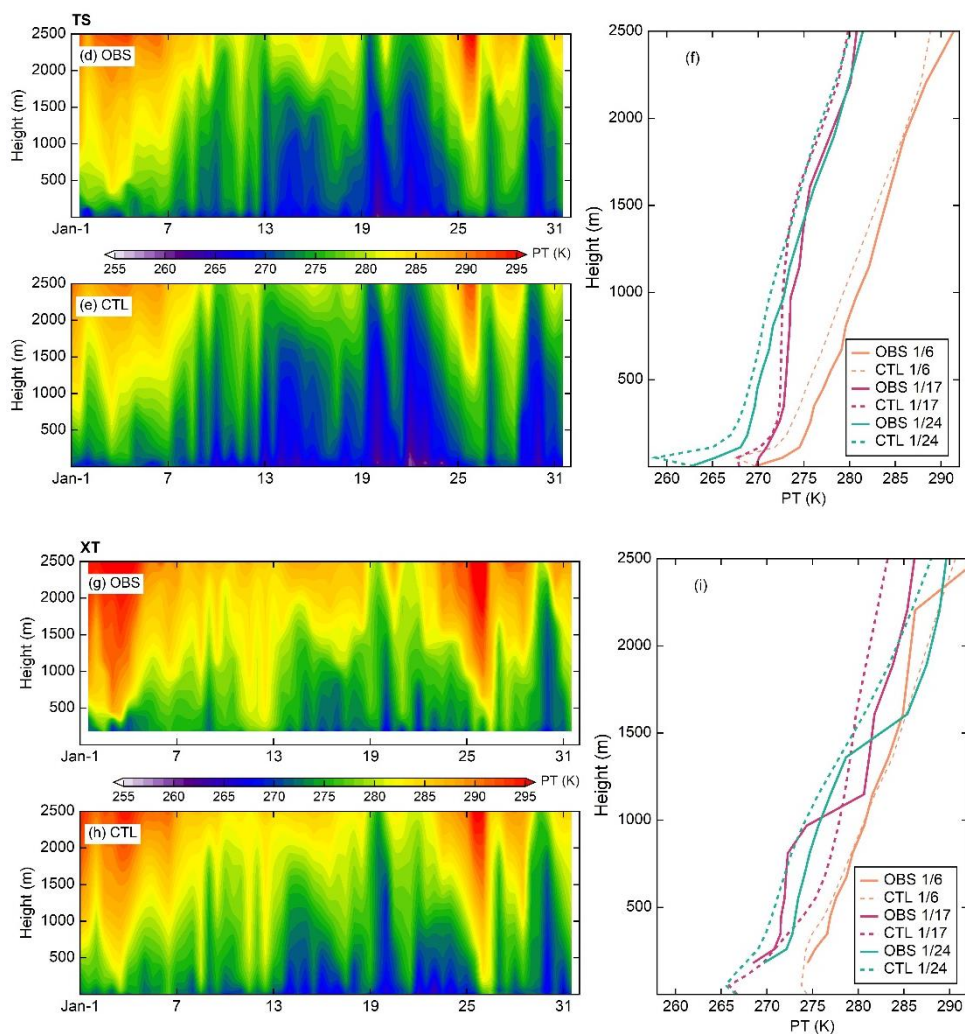


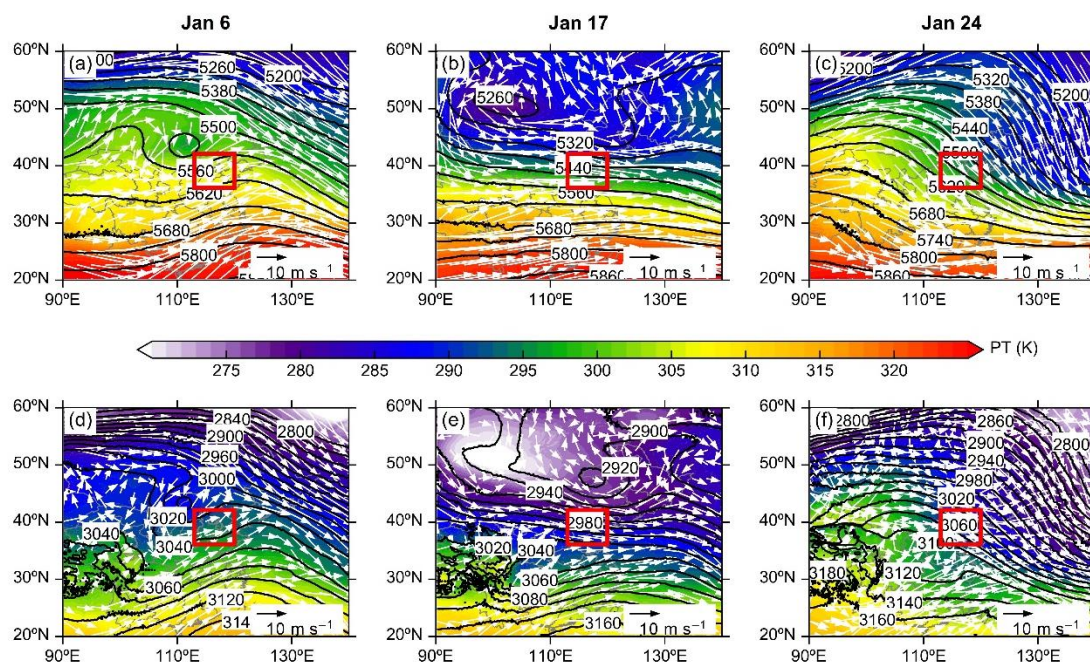
**Figure 3.** Vertical profiles of observed (OBS) and simulated (CTL) PT for (a–b) BJ, (d–e) TS, and (g–h) XT at 08:00 and 20:00 BJT in January 2017. c, f, and i denote the PT profiles for these three cities at 08:00 BJT on January 6, 17, and 24.

### 150 3.2 Weather situation background under haze pollution

Based on the distribution characteristics of pollutants in the BTH region and the good simulation performance of the model, the horizontal distribution of the upper, middle, lower atmosphere and surface circulation field in the pollution days was examined. First, the geopotential height (GH), PT, and wind vectors at the 500 and 700 hPa levels on January 6, 17, and 24 were discussed using the FNL data. Previous studies have shown that persistent pollution is influenced not only by the PBL and surface meteorology but also by the configuration of upper and low-level circulation systems (Miao et al., 2015; Wu et al., 2017). The circulation patterns across the BTH differed considerably during these three days (Fig. 4). On January 6, eastern China was in front of a weak north-south trough at 500 hPa, and the BTH region was controlled by southwest airflow



and a slight temperature gradient. On January 17, a zonal circulation dominated East Asia, and a zonal westerly airflow was in charge of the BTH region. On January 24, mainland China was dominated by a northeast-southwest high pressure ridge, and the BTH region was controlled by northwesterly airflow in front of this ridge. Moreover, the circulation patterns at 700 hPa were consistent with that at 500 hPa. All these synoptic conditions are generally considered to promote the deterioration of pollution since they impede the southward movement of cold air from the north and west and strengthen the downdraft (Wu et al., 2017; Zhang et al., 2019).



165 **Figure 4.** Distribution of GH (black line), PT (shading), and wind vectors (white arrow) at 500 and 700 hPa on January 6, 17, and 24.

Figure 5 displays the distribution of simulated GH, PT, and wind vectors at 850 hPa level on the three days. On January 6, most of the BTH region was between two weak high pressures. Influenced by the southwesterly and southeasterly winds, the warm and humid air masses from the south and the sea were brought to the central and southern BTH. The northern BTH was mainly controlled by low pressure to the northeast, and the northwesterly winds in the area were reduced due to the blockage of the Taihang and Yanshan Mountains. On January 17, the BTH region was between the low pressure in the northeast and the high pressure in the southwest, leaving most of BTH under the control of northwesterly winds. On January 24, eastern China was under the control of subtropical high pressure. The BTH region was located north of the subtropical high center, with westerly and southwesterly winds prevailing. At the same time, 850 hPa temperature decreased from southwest to northeast, and such a wind field is also conducive to bringing the warm and humid air masses from the south to BTH.



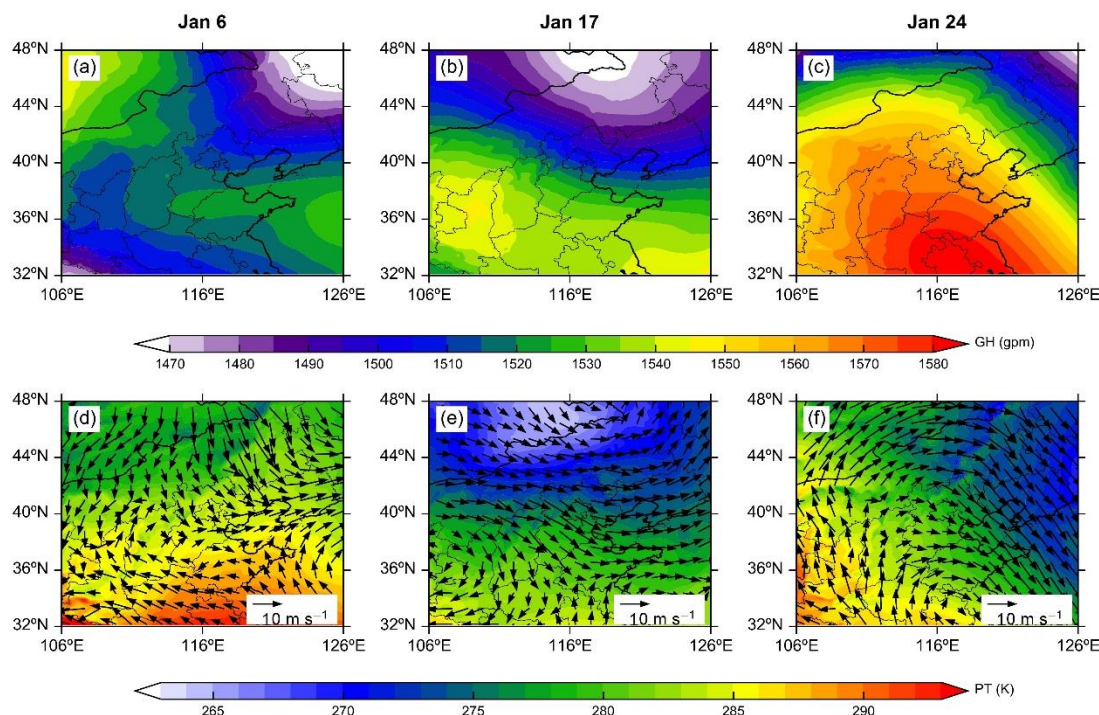
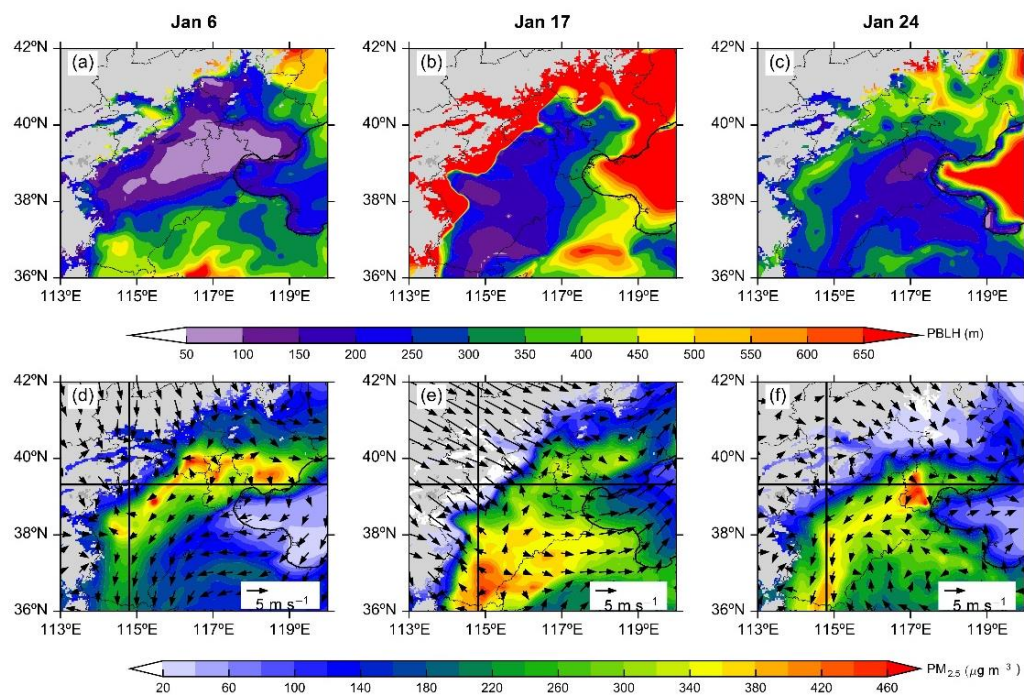


**Figure 5.** Distribution of simulated (CTL) GH (a–c), PT (d–f: shading), and wind vectors (d–f: black arrow) at 850 hPa on 180 January 6, 17, and 24.

The northerly or northwesterly airflow in the lower troposphere tends to form a sink motion on the leeward slope after being blocked by the Yanshan and Taihang Mountains, which will lead to a decrease in the height of the PBL (PBLH) and the wind speed in the plain of BTH region (Fig. 6). On the three days, the daily mean PBLH was generally below 300 m in the central and southern plains of BTH, and its low-value area corresponded well to the high-value area of near-surface PM<sub>2.5</sub> concentrations. Moreover, due to the disturbance of local circulation caused by the Yanshan and Taihang Mountains, the near-surface wind field showed different distribution characteristics from the lower troposphere with wind speeds below 2 m s<sup>-1</sup> in most areas. On January 6, high PM<sub>2.5</sub> concentrations were concentrated in eastern BTH, and a northeast-southwest transport channel was formed under the influence of northeasterly winds. On January 17, northwesterly winds prevailed in the northern Beijing area due to strong airflow in the lower troposphere. However, the blockage of the mountains made the airflow sharply weakened in the plain area after crossing the mountains, and formed subsidence and weak divergence, which led to a large accumulation of pollutants here. The distribution of wind fields in the plain of BTH on January 24 was similar to that on January 6, and there was also a pollution transport channel from southern Beijing to Xingtai area. 185 190



195 **Figure 6.** Distribution of simulated (CTL) daytime (09:00–16:00 BJT) PBLH (a–c), near-surface  $\text{PM}_{2.5}$  concentrations (d–f: shading), and wind vectors at 10 m (d–f: black arrow) on January 6, 17, and 24. The grey shading denotes the terrain height over 1000 m. The black lines indicate the location of the vertical cross-sections shown in Figures 7–10.

### 3.3 Influence of local circulations on pollutant distribution

Under these similar weak weather-scale systems, local circulation may dominate the distribution of pollutants and the development of haze. Figure 7 displays the daytime vertical circulation vectors and  $\text{PM}_{2.5}$  concentrations along the west-east (to the east of the Taihang Mountains) cross section and along the south-north (to the south of the border between the Taihang and Yanshan Mountains) cross section respectively on the three days. For the cross-section along west-east, the vertical circulation was similar on January 6 and 24: the westerly airflow sharply weakened after crossing the mountains, and the zonal wind speeds at low levels ( $< 500$  m, where the pollution was most severe) were mostly below  $2 \text{ m s}^{-1}$ ; the differential heating between the mountain slopes and the plains caused the atmosphere on the slopes to rise with relative heating and the atmosphere on the plains to sink with relative cooling, resulting in a weak clockwise local circulation between the eastern Taihang Mountains and the BTH plain (Fig. 7a, c). Pollutants accumulated in the PBL through this recirculation, and their concentration distribution was closely related to the scale and location of the circulation. Compared to January 24, the circulation was lower ( $< 300$  m) but more eastward (about  $119^\circ \text{ E}$ ) on January 6, so the high  $\text{PM}_{2.5}$  concentrations were concentrated at lower altitudes but more widely west-east. On January 17, although a sinking motion occurred within the PBL, the zonal wind speeds were larger throughout the layer compared to the other two days, mostly

200  
205  
210



215 ranging between 2 to  $5 \text{ m s}^{-1}$  (Fig. 7b). The stronger westerly winds made it relatively easy for pollutants to disperse  
eastward, thus the  $\text{PM}_{2.5}$  concentrations were lower than those on the other two days. For the cross-section along south-north,  
the  $\text{PM}_{2.5}$  concentrations on January 6 were significantly lower than those on January 17 and 24. On January 6, northeasterly  
winds prevailed near the surface of the center and southern BTH, and the pollutants were transported from northeast to  
southwest via this channel (Fig. 6d); the airflow over the mountains formed a whole layer of subsidence near  $38^\circ\text{N}$  (Fig. 7d),  
which inhibited the upward transport of pollutants; at the same time, there was a vertical local circulation at  $33\text{--}37^\circ\text{N}$ ,  
between 700 and 1500 m (Fig. 7d), which made pollutants recirculate in this region and not easily disperse to the outside.  
220 However, due to the high altitude of this circulation, its restrictions on pollutants were not as strong as the zonal circulations  
on January 6 (Fig. 7a) and 24 (Fig. 7c). On January 17, a wind convergence zone accompanied by sinking motion existed in  
the lower levels ( $< 1000 \text{ m}$ ) near  $37^\circ\text{N}$  (Fig. 7e). The combined effect of southerly and northerly winds made the pollutants  
difficult to disperse outward, thus accumulating locally. On January 24, a clockwise circulation was located between the  
southern slopes of the mountains and the plains north of  $35^\circ\text{N}$  (Fig. 7f), with its center at about 700 m; Southerly winds  
prevailed throughout the layer south of  $35^\circ\text{N}$ . Thus, air pollutants recirculated and accumulated by the superposition of the  
225 lower circulation and southerly winds.

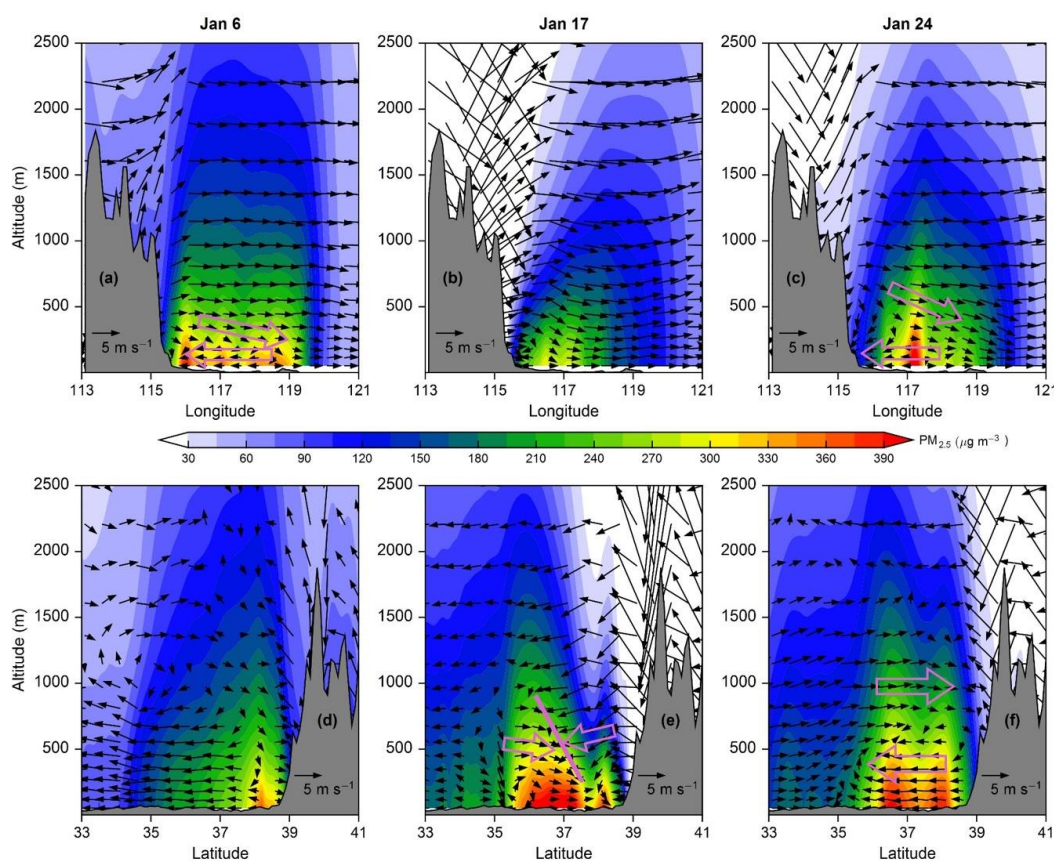




**Figure 7.** Vertical cross-section of simulated (CTL) wind field (a–c: zonal wind and 100 times of vertical velocity; d–f: meridional wind and 100 times of vertical velocity) and  $PM_{2.5}$  concentrations during daytime (09:00–16:00 BJT) on January 6, 17, and 24. Rose arrow indicates the direction of airflow, and rose line indicates the wind convergence line.

### 230 3.4 Amplification of local circulations on heavy haze by ARI

Given the considerable impact of local circulation on the distribution of air pollutants and the influence of ARI on the vertical structure of the PBL, it is necessary to further analyze the possible impacts of ARI on local. As shown in Figs. 8–11, the effects of ARI on circulations could be broadly classified into two types: strengthened local circulation and weakened horizontal transport. First, ARI significantly strengthened the vertical circulations on January 6 and 24, particularly for the zonal circulations: the high aerosol concentrations concentrated on the BTH plain during the daytime substantially cooled the lower atmosphere by absorbing and scattering solar radiation, and the widening difference in atmospheric heating between the mountain slopes and the BTH plain led to a simultaneous strengthening of westerly winds in the upper level and easterly winds in the lower level (Fig. 8a, c). On January 6, between the eastern Taihang Mountains and  $119^{\circ}E$ , ARI increased the westerly winds (300–800 m) and the easterly winds ( $< 300$  m) by  $0.8$  and  $0.3$   $m\ s^{-1}$ , respectively. On January 24, ARI increased the westerly winds (400–900 m) between the eastern Taihang Mountains and  $119^{\circ}E$  by  $0.7$   $m\ s^{-1}$ , and easterly winds ( $< 300$  m) west of  $117^{\circ}E$  by  $0.2$   $m\ s^{-1}$ ; at the same time, ARI decreased the westerly winds ( $< 300$  m) between  $117$  and  $119^{\circ}E$  by  $0.3$   $m\ s^{-1}$ , which hindered the eastward transport of aerosols. Moreover, ARI could change the altitude of circulation. On January 6, ARI shifted the vertical circulation downward by about 100 m according to the wind speed minimum and the height of the wind shear (Fig. 10a, d). The stronger and lower vertical circulation caused further accumulation of pollutants in the lower level, which then led to substantial cooling of the lower atmosphere (Fig. 8d, f) and weak vertical turbulent diffusion (Fig. 8g, i). ARI also strengthened the meridional circulations on January 6 and 24, although it did not cause the same downshift as the zonal circulations: Due to the ARI effect, the southerly winds in the upper level and the northerly winds in the lower level were strengthened simultaneously (Fig. 9a, c); the strengthened vertical circulation in this local area likewise traps the pollutants in the limited space, which further cooled atmosphere (Fig. 9d, f) and weakened turbulent diffusion (Fig. 9g, i) in lower atmosphere.

Second, ARI weakened the horizontal transport on January 17. For the relatively lightly polluted northern BTH, ARI weakened the westerly winds below 300 m and east of  $117^{\circ}E$  (Fig. 8b), with a maximum wind speed reduction of  $1$   $m\ s^{-1}$ . In addition, ARI enhanced the sinking of airflow near  $116^{\circ}E$ , promoting the accumulation of aerosols in the lower layer. For the heavily severe polluted southern BTH, ARI enhanced the wind convergence zone near  $37^{\circ}N$  (Fig. 11b) by simultaneously strengthening the southerly winds south of the convergence line and the northerly winds north of the convergence line (Fig. 9b). At the same time, ARI pushed this convergence line northward, causing southerly winds to prevail below 200 m over the plain. Pollutants could not be transported northward due to the blockage of the Yanshan Mountains. Both of these weakened the horizontal transport of pollutants, and thus the highly concentrated pollutants led to

cooling of the lower atmosphere (Figs. 8e and 9e) and weakening of the vertical turbulent motion (Figs. 8h and 9h), just like  
260 January 6 and 24.

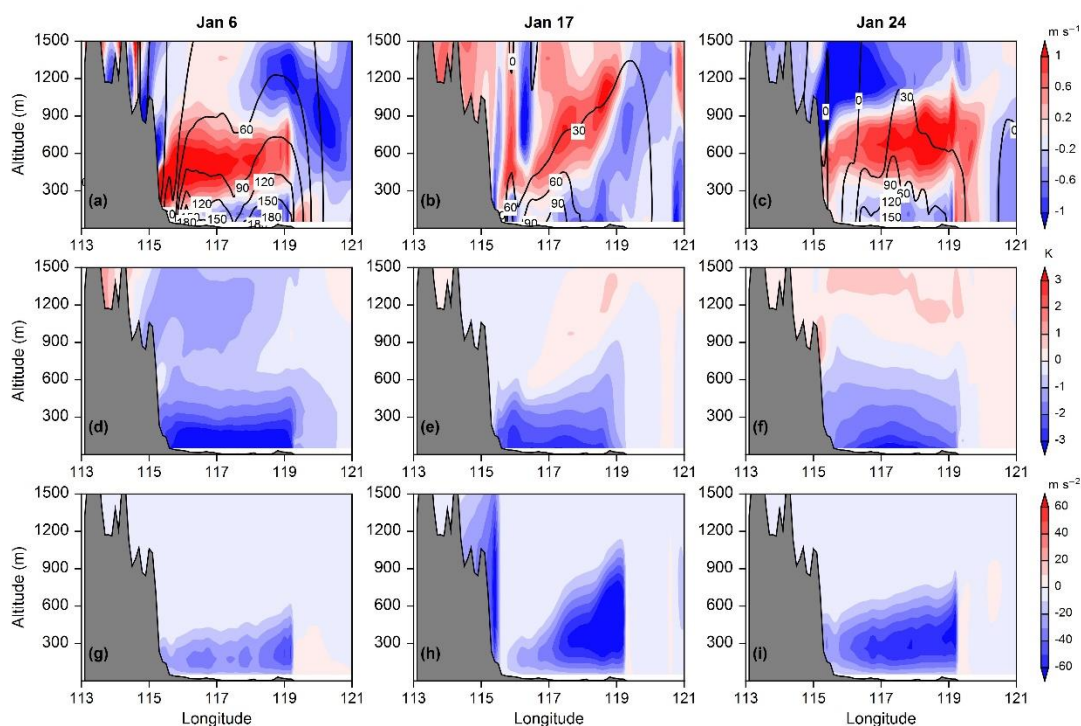
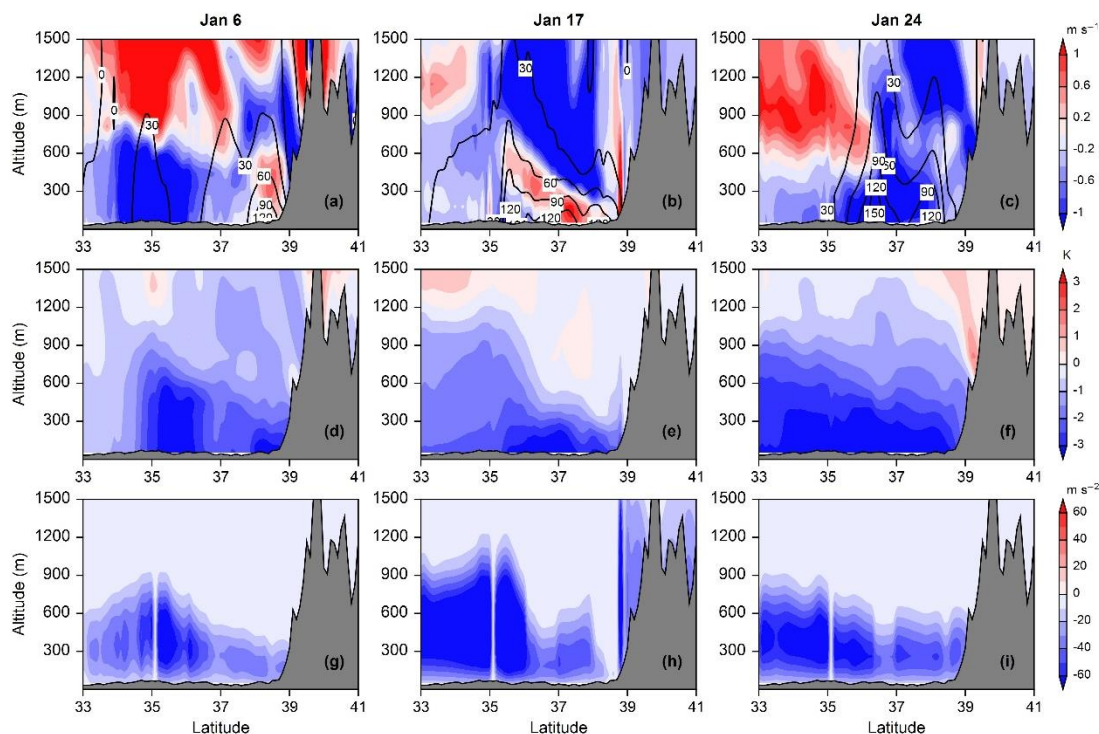
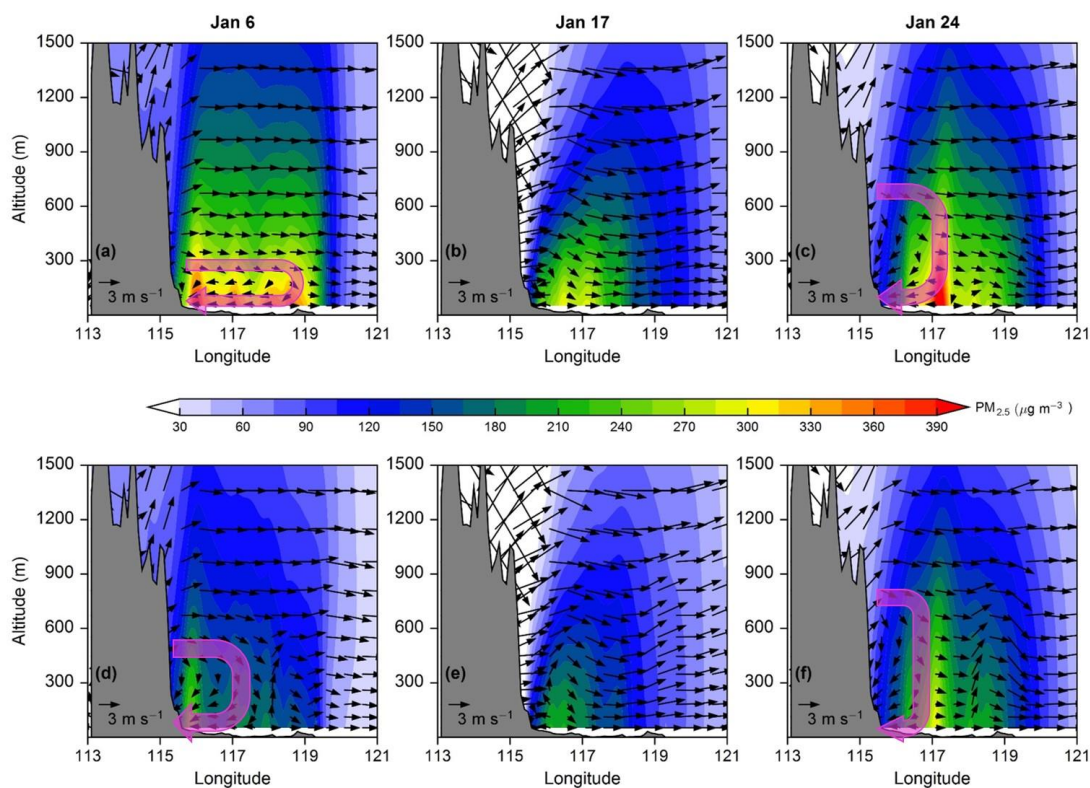


**Figure 8.** Vertical cross-section of simulated (a–c) zonal wind (shading) and  $\text{PM}_{2.5}$  concentration (contour:  $\mu\text{g m}^{-3}$ ), (d–f) PT, and (g–i) vertical turbulent diffusion coefficient differences (CTL–EXP) induced by aerosol–radiation feedbacks during daytime (09:00–16:00 BJT) on January 6, 17, and 24.



265

**Figure 9.** Vertical cross-section of simulated meridional wind (a–c: shading), PM<sub>2.5</sub> concentration (a–c: contours,  $\mu\text{g m}^{-3}$ ), PT (d–f), and vertical turbulent diffusion coefficient differences (CTL–EXP) induced by aerosol–radiation feedbacks during daytime (09:00–16:00 BJT) on January 6, 17, and 24.



270 **Figure 10.** Vertical cross-section of simulated wind field (zonal wind and 100 times of vertical velocity) and PM<sub>2.5</sub> concentrations from (a–c) CTL and (d–f) EXP during daytime (09:00–16:00 BJT) on January 6, 17, and 24. Rose arrow indicates the general location of the vertical circulation.

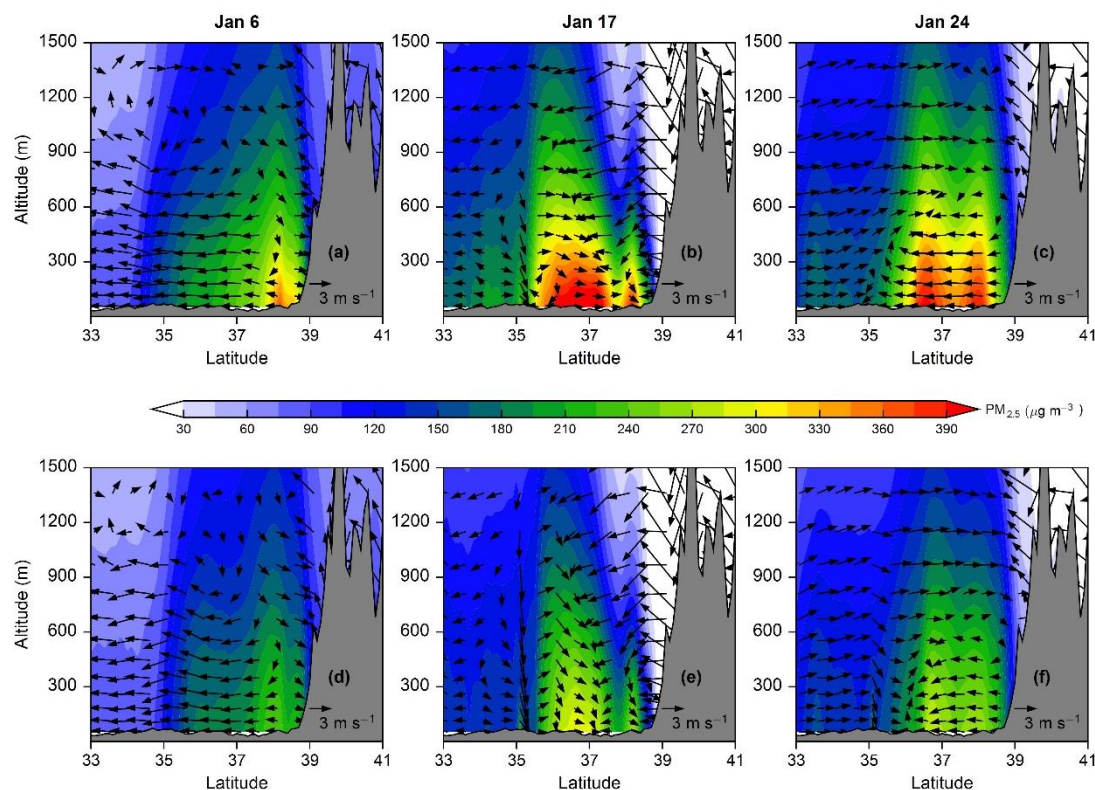


**Figure 11.** Vertical cross-section of simulated wind field (meridional wind and 100 times of vertical velocity) and  $PM_{2.5}$  concentrations from (a–c) CTL and (d–f) EXP during daytime (09:00–16:00 BJT) on January 6, 17, and 24.

#### 4 Conclusions

In this study, the link between aerosol, local vertical circulation, and heavy haze pollution in the BTH plain in winter was investigated, based on surface and sounding observations and simulation experiments by the atmospheric chemistry model GRAPES\_Meso5.1/CUACE in January 2017.

280 From synoptic perspective, the appropriate configurations of the upper, middle, and lower levels provided favorable conditions for the accumulation of pollutants. During the haze pollution, the BTH region was mainly controlled by the zonal westerly airflow or northwesterly airflow in front of the high pressure ridge at the upper and middle levels, and the most polluted central and southern BTH was often dominated by the southwesterly winds at the lower levels; at the same time, the blockage of the Taihang and Yanshan Mountains significantly weakened airflow from the west and north, while hindering  
285 the northward and westward transport of pollutants.

Under these unfavorable synoptic conditions, the typical local circulation induced by the mountainous topography played a key role in the heavy haze pollution. During the daytime on the selected pollution days, the differential heating induced by





mountainous topography led to the formation of local closed vertical circulation and wind convergence in the lower atmosphere between the mountain slopes and the BTH plain, which was not conducive to the vertical diffusion and horizontal transport of the pollutants and led to their recirculation and accumulation in local areas. Both the size and location of the vertical circulation played an important role in the pollutant distribution. A smaller-scale, lower-altitude circulation could constrain near-surface pollutants to a more limited area. More importantly, the superposition of the ARI mechanism and local circulation could significantly aggravate haze pollution. According to the simulation results of this study, ARI mainly amplified the impacts of local vertical circulation on haze in the two ways: strengthening local circulation and weakening horizontal transport. For the clockwise vertical circulation along west-east, ARI not only strengthened the upper westerly winds and the lower easterly winds, but also pressed the circulation down to the lower atmosphere; for the wind convergence formed along south-north, ARI strengthened the southerly and northerly winds on both sides of the convergence line, and made the convergence line move northward. Through the above two pathways, ARI amplified the inhibitory of local circulation on vertical diffusion and horizontal transport, trapping pollutants in a more limited space. With the superposition of ARI and local circulation, aerosols accumulated rapidly in the lower atmosphere, which led to more stable atmospheric stratification and subsequent deterioration of haze pollution.

#### **Data availability**

All raw data can be provided by the corresponding authors upon request.

#### **Author contribution**

HW and XZ conceived the idea; YP and HW designed the experiment; YP ran the model and wrote the manuscript draft; ZL and WZ provided the observation data; YP, SL, and CH analysed the data; YP, HW, and HC reviewed and edited the manuscript.

#### **Competing interests**

The authors declare that they have no conflict of interest.

#### **Financial support**

This work was supported by the NSFC Major Project (42090030), the National Key Research and Development Program of China (2019YFC0214601), and the NSFC for Distinguished Young Scholars (41825011).



## References

- Chen, D. H., Xue, J. S., Yang, X. S., Zhang, H. L., Shen, X. S., Hu, J. L., Wang, Y., Ji, L. R., and Chen, J. B.: New  
315 generation of multi-scale NWP system (GRAPES): general scientific design, *Chin. Sci. Bull.*, 53, 3433–3445,  
<https://doi.org/10.1007/s11434-008-0494-z>, 2008.
- Chen, Y., Zhao, C., Zhang, Q., Deng, Z., Huang, M., and Ma, X.: Aircraft study of mountain chimney effect of Beijing,  
China, *J. Geophys. Res.*, 114, D08306, <https://doi.org/10.1029/2008JD010610>, 2009.
- Chou, M. D., Suarez, M. J., Ho, C. H., Yan, M. M. H., and Lee, K. T.: Parameterizations for cloud overlapping and  
320 shortwave single-scattering properties for use in general circulation and cloud ensemble models, *J. Clim.*, 11, 202–214,  
1998.
- Ding, A. J., Huang, X., Nie, W., Sun, J. N., Kerminen, V. M., Petäjä T., Su, H., Cheng, Y. F., Yang, X.-Q., Wang, M. H.,  
Chi, X. G., Wang, J. P., Virkkula, A., Guo, W. D., Yuan, J., Wang, S. Y., Zhang, R. J., Wu, Y. F., Song, Y., Zhu, T.,  
Zilitinkevich, S., Kulmala, M., and Fu, C. B.: Enhanced haze pollution by black carbon in megacities in China,  
325 *Geophys. Res. Lett.*, 43(6), 2873–2879, <https://doi.org/10.1002/2016GL067745>, 2016.
- Ek, M. B., Mitchell, K. E., Lin, Y., Rogers, E., Grunmann, P., Koren, V., Gayno, G., and Tarpley, J. D.: Implementation of  
Noah land surface model advances in the National Centres for Environmental Prediction operational mesoscale Eta  
model, *J. Geophys. Res.*, 108 (D22), 8851, <https://doi.org/10.1029/2002JD003296>, 2003.
- Fu, G. Q., Xu, W. Y., Yang, R. F., Li, J. B., and Zhao, C. S.: The distribution and trends of fog and haze in the North China  
330 Plain over the past 30 years, *Atmos. Chem. Phys.*, 14, 11949–11958, <https://doi.org/10.5194/acp-14-11949-2014>, 2014.
- Gao, M., Liu, Z., Wang, Y., Lu, X., Ji, D., and Wang, L.: Distinguishing the roles of meteorology, emission control measures,  
regional transport, and co-benefits of reduced aerosol feedback in “APEC” Blue, *Atmos. Environ.*, 167, 476–486,  
<https://doi.org/10.1016/j.atmosenv.2017.08.054>, 2017.
- Gong, S. L., and Zhang, X. Y.: CUACE/Dust – an integrated system of observation and modeling systems for operational  
335 dust forecasting in Asia, *Atmos. Chem. Phys.*, 8, 2333–2340, 2008.
- Hong, S. Y., and Pan, H. L.: Nonlocal boundary layer vertical diffusion in a medium-range forecast model, *Mon. Weather  
Rev.*, 124, 2322, 1996.
- Huang, X., Ding, A., Wang, Z., Ding, K., Gao, J., Chai, F., and Fu, C.: Amplified transboundary transport of haze by  
aerosol–boundary layer interaction in China, *Nat. Geosci.*, 13, 428–434, <https://doi.org/10.1038/s41561-020-0583-4>,  
340 2020.
- Huang, X., Wang, Z., and Ding, A.: Impact of aerosol-PBL interaction on haze pollution: Multiyear observational evidences  
in North China, *Geophys. Res. Lett.*, 45(16), 8596–8603, <https://doi.org/10.1029/2018GL079239>, 2018.
- Kain, J. S.: The Kain-Fritsch convective parameterization: An update, *J. Appl. Meteor.*, 43, 170–181, 2004.



- Mlawer, E. J., Taubman, S. J., Brown, P. D., Iacono, M. J., and Clough, S. A.: Radiative transfer for inhomogeneous  
345 atmosphere: RRTM, a validated correlated-k model for the longwave, *J. Geophys. Res.*, 102, 16663–16682,  
<https://doi.org/10.1029/97JD00237>, 1997.
- Li, Z., Guo, J., Ding, A., Liao, H., Liu, J., Sun, Y., Wang, T., Xue, H., Zhang, H., and Zhu, B.: Aerosol and boundary-layer  
interactions and impact on air quality, *Natl. Sci. Rev.*, 4, 810–833, <https://doi.org/10.1093/nsr/nwx117>, 2017.
- Liu, Q., Jia, X., Quan, J., Li, J., Li, X., Wu, Y., Chen, D., Wang, Z., and Liu, Y.: New positive feedback mechanism between  
350 boundary layer meteorology and secondary aerosol formation during severe haze events, *Sci. Rep.*, 8, 6095,  
<https://doi.org/10.1038/s41598-018-24366-3>, 2018.
- Liu, S., Liu, Z., Li, J., Wang, Y., Ma, Y., Sheng, L., Liu, H., Liang, F., Xin, G., and Wang, J.: Numerical simulation for the  
coupling effect of local atmospheric circulations over the area of Beijing, Tianjin and Hebei Province, *Sci. China Ser.  
D-Earth Sci.* 52, 382–392, <https://doi.org/10.1007/s11430-009-0030-2>, 2009.
- 355 Lo, J. C. F., Lau, A. K. H., Fung, J. C. H. and Chen, F.: Investigation of enhanced cross-city transport and trapping of air  
pollutants by coastal and urban land-sea breeze circulations, *J. Geophys. Res.*, 111, D14104,  
<https://doi.org/10.1029/2005JD006837>, 2006.
- Miao, Y., Che, H., Zhang, X., and Liu, S.: Integrated impacts of synoptic forcing and aerosol radiative effect on boundary  
layer and pollution in the Beijing–Tianjin–Hebei region, China, *Atmos. Chem. Phys.*, 20, 5899–5909,  
360 <https://doi.org/10.5194/acp-20-5899-2020>, 2020.
- Miao, Y., Li, J., Miao, S., Che, H., Wang, Y., Zhang, X., Zhu, R., and Liu, S.: Interaction between planetary boundary layer  
and PM<sub>2.5</sub> pollution in megacities in China: a Review, *Curr. Pollut. Rep.*, 5(4), 261–271,  
<https://doi.org/10.1007/s40726-019-00124-5>, 2019.
- Miao, Y., Liu, S., Zheng, Y., Wang, S., Chen, B., Zheng, H., and Zhao, J.: Numerical study of the effects of local  
365 atmospheric circulations on a pollution event over Beijing–Tianjin–Hebei, China, *J. Environ. Sci.* 30, 9–20,  
<http://dx.doi.org/10.1016/j.jes.2014.08.025>, 2015.
- Peng, Y., Wang, H., Hou, M., Jiang, T., Zhang, M., Zhao, T., and Che, H.: Improved method of visibility parameterization  
focusing on high humidity and aerosol concentrations during fog–haze events: Application in the GRAPES\_CAUCE  
model in Jing-Jin-Ji, China, *Atmos. Environ.*, 222, 117139, <https://doi.org/10.1016/j.atmosenv.2019.117139>, 2020.
- 370 Peng, Y., Wang, H., Zhang, X., Zhao, T., Jiang, T., Che, H., Zhang, X., Zhang, W., and Liu, Z.: Impacts of PBL schemes on  
PM<sub>2.5</sub> simulation and their responses to aerosol-radiation feedback in GRAPES\_CUACE model during severe haze  
episodes in Jing-Jin-Ji, China, *Atmos. Res.* 248, 105268, <https://doi.org/10.1016/j.atmosres.2020.105268>, 2021.
- Peng, Y., Wang, H., Zhang, X., Zheng, Y., Zhang, X., Zhang, W., Liu, Z., Gui, K., Liu, H., Wang, Y., and Che, H.: Aerosol-  
radiation interaction in the operational atmospheric chemistry model GRAPES\_Meso5.1/CUACE and its impacts on  
375 mesoscale NWP in Beijing-Tianjin-Hebei, China, *Atmos. Res.*, under review.



- Quan, J., Dou, Y., Zhao, X., Liu, Q., Sun, Z., Pan, Y., Jia, X., Cheng, Z., Ma, P., Su, J., Xin, J., and Liu, Y.: Regional atmospheric pollutant transport mechanisms over the North China Plain driven by topography and planetary boundary layer processes, *Atmos. Environ.*, 221, 117098, <https://doi.org/10.1016/j.atmosenv.2019.117098>, 2020.
- 380 Quan, J., Gao, Y., Zhang, Q., Tie, X., Cao, J., Han, S., Meng, J., Chen, P., and Zhao, D.: Evolution of planetary boundary layer under different weather conditions, and its impact on aerosol concentrations, *Particuology*, 11(1): 34–40, <http://dx.doi.org/10.1016/j.partic.2012.04.005>, 2013.
- Stockwell, W. R., Middleton, P., Chang, J. S., and Tang, X.: The second generation regional acid deposition model chemical mechanism for regional air quality modeling, *J. Geophys. Res.*, 95, 16343–16367, <https://doi.org/10.1029/JD095iD10p16343>, 1990.
- 385 Sun, Y., Song, T., Tang, G., and Wang, Y.: The vertical distribution of PM<sub>2.5</sub> and boundary-layer structure during summer haze in Beijing, *Atmos. Environ.*, 74, 413–421, <https://doi.org/10.1016/j.atmosenv.2013.03.011>, 2013.
- Thompson, G., Field, P. R., Rasmussen, R. M., and Hall, W. D.: Explicit Forecasts of Winter Precipitation Using an Improved Bulk Microphysics Scheme. Part II: Implementation of a New Snow Parameterization, *Mon. Weather Rev.*, 136, 5095–5115, <https://doi.org/10.1175/2008MWR2387.1>, 2008.
- 390 Wang, D., Jiang, B., Lin, W., and Gu, F.: Effects of aerosol-radiation feedback and topography during an air pollution event over the North China Plain during December 2017, *Atmos. Pollut. Res.*, <https://doi.org/10.1016/j.apr.2018.10.006>, 2019.
- Wang, H., Gong, S., Zhang, H., Chen, Y., Shen, X., Chen, D., Xue, J., Shen, Y., Wu, X., and Jin, Z.: A new-generation sand and dust storm forecasting system GRAPES\_CUACE/Dust: Model development, verification and numerical simulation, *Chin. Sci. Bull.*, 55(7), 635–649, <https://doi.org/10.1007/s11434-009-0481-z>, 2010.
- 395 Wang, H., Peng, Y., Zhang, X., Liu, H., Zhang, M., Che, H., Cheng, Y., and Zheng, Y.: Contributions to the explosive growth of PM<sub>2.5</sub> mass due to aerosol–radiation feedback and decrease in turbulent diffusion during a red alert heavy haze in Beijing–Tianjin–Hebei, China. *Atmos. Chem. Phys.* 18, 17717–17733, <https://doi.org/10.5194/acp-18-17717-2018>, 2018.
- 400 Wang, H., Shi, G. Y., Zhang, X. Y., Gong, S. L., Tan, S. C., Chen, B., Che, H. Z., and Li, T.: Mesoscale modelling study of the interactions between aerosols and PBL meteorology during a haze episode in China Jing–Jin–Ji and its near surrounding region – Part 2: Aerosols' radiative feedback effects, *Atmos. Chem. Phys.*, 15, 3277–3287, <https://doi.org/10.5194/acp-15-3277-2015>, 2015b.
- Wang, H., Xue, M., Zhang, X. Y., Liu, H. L., Zhou, C. H., Tan, S. C., Che, H. Z., Chen, B., and Li, T.: Mesoscale modeling study of the interactions between aerosols and PBL meteorology during a haze episode in Jing–Jin–Ji (China) and its nearby surrounding region – Part 1: Aerosol distributions and meteorological features, *Atmos. Chem. Phys.*, 15, 3257–3275, <https://doi.org/10.5194/acp-15-3257-2015>, 2015a.
- 405 Wang, H., Zhang, X. Y., Wang, P., Peng, Y., Zhang, W., Liu, Z., Han, C., Li, S., Wang, Y., Che, H., Huang, L., Liu, H., Zhang, L., Zhou, C., Ma, Z., Chen, F., Ma, X., Wu, X., Zhang, B., and Shen, X.: Chemistry-Weather Interacted Model



- 410 System GRAPES\_Meso5.1/CUACE CW V1.0: Development, Evaluation and Application in Better Haze-fog  
Prediction in China, *J. Adv. Model. Earth Syst.*, under review.
- Wu, P., Ding, Y. H., and Liu, Y. J.: Atmospheric circulation and dynamic mechanism for persistent haze events in the  
Beijing–Tianjin–Hebei region, *Adv. Atmos. Sci.*, 34(4), 429–440, <https://doi.org/10.1007/s00376-016-6158-z>, 2017.
- Zhang, B., Wang, Y., and Hao, J.: Simulating aerosol–radiation–cloud feedbacks on meteorology and air quality over eastern  
China under severe haze conditions in winter, *Atmos. Chem. Phys.*, 15, 2387–2404, [https://doi.org/10.5194/acp-15-](https://doi.org/10.5194/acp-15-2387-2015)  
415 [2387-2015](https://doi.org/10.5194/acp-15-2387-2015), 2015.
- Zhang, D., and Anthes, R. A.: A high-resolution model of the planetary boundary layer—sensitivity tests and comparisons  
with SESAME-79 data, *J. Appl. Meteorol.*, 21, 1594–1609, 1982.
- Zhang, Q., Zheng, Y., Tong, D., Shao, M., Wang, S., Zhang, Y., Xu, X., Wang, J., He, H., Liu, W., Ding, Y., Lei, Y., Li, J.,  
Wang, Z., Zhang, X., Wang, Y., Cheng, J., Liu, Y., Shi, Q., and Hao, J.: Drivers of improved PM<sub>2.5</sub> air quality in  
420 China from 2013 to 2017, *P. Nat. Acad. Sci. USA*, 116, 201907956, <https://doi.org/10.1073/pnas.1907956116>, 2019.
- Zhang, W., Wang, H., Zhang, X., Peng, Y., Zhong, J., Wang, Y., and Zhao, Y.: Evaluating the contributions of changed  
meteorological conditions and emission to substantial reductions of PM<sub>2.5</sub> concentration from winter 2016 to 2017 in  
Central and Eastern China, *Sci. Total Environ.*, 136892, <https://doi.org/10.1016/j.scitotenv.2020.136892>, 2020.
- Zhang, X., Xu, X., Ding, Y., Liu, Y., Zhang, H., Wang, Y., and Zhong, J.: The impact of meteorological changes from 2013  
425 to 2017 on PM<sub>2.5</sub> mass reduction in key regions in China, *Sci. China Earth Sci.*, 62: 1885–1902,  
<https://doi.org/10.1007/s11430-019-9343-3>, 2019.
- Zhang, Z., Xu, X., Qiao, L., Gong, D., Kim, S.-J., Wang, Y., and Mao, R.: Numerical simulations of the effects of regional  
topography on haze pollution in Beijing, *Sci. Rep.*, 8, 5504, <https://doi.org/10.1038/s41598-018-23880-8>, 2018.
- Zhao, B., Liou, K.-N., Gu, Y., Li, Q., Jiang, J. H., Su, H., He, C. L., Tseng, H. L., Wang, S. X., Liu, R., Qi, L., Lee, W. L.,  
430 and Hao, J. M.: Enhanced PM<sub>2.5</sub> pollution in China due to aerosol–cloud interactions, *Sci. Rep.*, 7, 4453,  
<https://doi.org/10.1038/s41598-017-04096-8>, 2017.
- Zheng, B., Tong, D., Li, M., Liu, F., Hong, C., Geng, G., Li, H., Li, X., Peng, L., Qi, J., Yan, L., Zhang, Y., Zhao, H., Zheng,  
Y., He, K., and Zhang, Q.: Trends in China's anthropogenic emissions since 2010 as the consequence of clean air  
actions, *Atmos. Chem. Phys.*, 18, 14095–14111, <https://doi.org/10.5194/acp-18-14095-2018>, 2018.
- 435 Zhong, J., Zhang, X., Dong, Y., Wang, Y., Liu, C., Wang, J., Zhang, Y., and Che, H.: Feedback effects of boundary-layer  
meteorological factors on cumulative explosive growth of PM<sub>2.5</sub> during winter heavy pollution episodes in Beijing  
from 2013 to 2016, *Atmos. Chem. Phys.*, 18, 247–258, <https://doi.org/10.5194/acp-18-247-2018>, 2018b.
- Zhong, J., Zhang, X., Wang, Y., Liu, C., Dong, Y.: Heavy aerosol pollution episodes in winter Beijing enhanced by radiative  
cooling effects of aerosols, *Atmos. Res.*, 209, 59–64, <https://doi.org/10.1016/j.atmosres.2018.03.011>, 2018a.